REAL-TIME MONITORING of WELD POOL during GTAW using INFRA-RED THERMOGRAPHY and analysis of Infra-Red thermal images

M. Vasudevan, N. Chandrasekhar, V. Maduraimuthu, A.K. Bhaduri and B. Raj

ABSTRACT

Real-time monitoring of the weld pool using infra-red (IR) thermography during gas tungsten arc (GTA) welding is gaining importance due to the requirements for on-line monitoring and control of the welding process. To facilitate real-time monitoring of the weld pool, a computer-controlled GTA welding machine with sensing of the weld pool using IR camera has been developed. The IR camera, mounted on the torch assembly, monitors the molten pool and the surface temperature distribution surrounding the weld pool during GTA welding. Temperature profiles were measured on the plates using thermocouples in combination with IR thermography to determine the emissivity of the plate surface. GTA welding was carried out on 3 mm-thick 316LN stainless steel (SS) plates under different welding conditions. IR thermal images were acquired on-line and analysed. A linear relationship was obtained between the thermal bead width, determined by line-scan analysis technique, and the actual bead width, measured by cross-sectional optical microscopy. The computed macroscopic temperature gradient and the actual of weld bead depth of penetration showed an inverse relationship. Full-frame analysis was carried out to estimate the surface temperature distribution for square-butt weld joints. For 316LN SS weld joints, IR thermal signatures were acquired for various weld defects, such as lack of fusion, lack of penetration and tungsten inclusions, for use as reference signatures for on-line monitoring during GTA welding.

IIW-Thesaurus keywords: Defects; Imaging; Infrared; Lack of fusion; Penetration defects; Thermography; Visual inspection; Welded joints.

1 Introduction

In recent years there has been considerable advancement in automation of welding processes using intelligent methodologies to facilitate on-line process monitoring and control, which can also be used for remote repair welding applications. Intelligent automation of gas tungsten arc (GTA) welding involves development of computer-based monitoring and control software with Human Machine Interface (HMI) that enables powerful, flexible, and user-friendly operator interface by bringing together all displays and functions needed for on-line monitoring and control of the welding machine. The HMI system integrates system operation at a single level and it gives the operator good visualization.

The HMI monitors and controls the servo and stepper motors and process parameters of the GTA welding machine as per standard program, as well as experimental requirements with the help of interfaced Galil motion controller and Programmable Logic Controller (PLC). The HMI tracks and records the process parameters of welding, such as voltage, current, jog speed, current axis value, of the welding machine. The HMI sends commands to the Galil and PLC for controlling the jogging, point-to-point positioning, vector positioning, multiple move sequence, wire-feeder up and down movement, arc voltage controller up and down movement, gas purge, homing the machine (i.e. to keep the machine at zero coordinates on all axes by mechanical reference so that the machine always starts from zero coordinates), cycle start and controls the torch assembly by setting the parameter into Galil motion control module and PLC. Visual basic software has been developed and interfaced with the PLC and Galil multi-axis motion control, by serial and Ethernet communication. In this way, a computer-operated fully automated GTA welding machine with HMI has been developed and integrated to facilitate the entire operation and control of the machine by a computer.

Also, a computer-based multi-channel data-acquisition system, employing a RS485 network, has also been developed for validating temperature measurements at various locations along the entire length on the plate surface close to the weld using C-type thermocouples. For this purpose, Visual Basic software has been developed to acquire and record temperatures measured by temperature indicators as a function of time [1].

In order to monitor and control the welding operations for producing quality welds in non-accessible areas, sensors capable of monitoring and controlling the welding process

Doc. IIW-2044, recommended for publication by Commission V "Quality Control and Quality Assurance of Welded Products."

is required to be incorporated into the robot. The significant advances in cameras in recent years have made possible the development of vision sensors for real-time monitoring and control of arc welding processes. Vision sensors have been used to monitor the seam position, weld pool width and depth of penetration in arc welding processes [2-4]. Among the vision sensors, infrared (IR) sensing is a natural choice for weld process monitoring, as welding is inherently a thermal processing method. Infrared sensing for weld process monitoring has been used by many researchers [3, 5-9]. IR sensing can also be used for detecting the occurrence of various weld defects during welding as they are known to cause perturbations in the surface temperature distributions of the plate being welded. The main advantage of IR sensing is its ability to monitor several weld parameters simultaneously. However, the use of IR thermography for quantitative temperature measurements in GTA welding is limited by difficulties in handling the surface emissivity variations, and the reflected radiation from the arc light and the hot tungsten electrode during welding. Therefore, a number of issues must be addressed when using IR thermography for real-time imaging of the weld pool during GTA welding.

In GTA welding, arc radiation occurs in the spectral range of 0.34 and 1.8 μm, while for wavelengths greater than 2 μm the weld radiation is greater in magnitude than the arc energy [10]. Thus, it is possible to improve the image quality acquired by an IR camera by filtering method and this now being commonly followed to minimize the interference from radiant reflection of the arc and the electrode. Filters selectively pass the desired wavelengths of IR radiation to the detector while attenuating the unwanted wavelengths that degrade the image quality. Bicknell [11] improved the IR image quality by using high-pass and band-pass filters. Farson [12] used a band-pass filter and shield to weaken the arc and electrode interference from the IR thermal radiation in GTA welding. The accuracy of the measurement of the surface temperature distributions of the plate during welding using the IR camera depends on the emissivity of the plate, which in turn is highly dependent on the surface condition of the plate. The surface emissivity increases during cooling and oxidation and hence, it is difficult to measure the actual emissivity during the cooling phase. As emissivity is a function of temperature, variations in the surface emissivity of the plate needs to be experimentally quantified.

The objectives of the present investigations are as follows.

1. Apply IR sensing in real-time to monitor the molten weld pool and the surface temperature distribution surrounding the weld pool during GTA welding of 316LN stainless steel (SS) plate.
2. Relate the weld bead width and depth of penetration to the measured surface temperature distributions.
3. Compare the actual weld bead width and depth of penetration with the thermal bead width and the macroscopic temperature gradients computed from line-scan analysis of the IR thermal image.
4. Estimate the surface temperature distribution for square-butt weld joints from IR thermal images.
5. Acquire and record IR thermal signature images for weld joints with and without weld defects.

2 Experimental

The experimental set-up used for real-time monitoring of the GTA welding process using an infrared (IR) camera is shown in Figure 1. The IR camera is mounted on the torch assembly and moves behind the torch at the welding speed to capture instantaneous images of the weld pool and the surrounding area of the plate being welded. The IR thermography system used is an ALTAIR workstation that comprises a JADE MWIR camera, FG9800 digital PCI frame grabber and ALTAIR software for image acquisition and processing. The JADE MWIR broad-band camera uses a high quantum efficiency focal plane array LnSb detector that is cooled by a high reliability Stirling cooler and provides images of high sensitivity in the wavelength range of 1.5-5.1 μm. The IR camera uses a high-pass band filter that permits only a portion of the emitted energy in the wavelength range of 4.99-5.10 μm, thereby minimizing the interference from arc light and hot tungsten electrode on the image quality. This IR camera with high-pass band filter is capable of measuring temperatures in the range 200-1 500 °C with an accuracy of ± 2 % over the entire range. Each scan of the camera is transferred as a frame consisting of 320 × 240 discrete intensity measurements at 50 frames per second. The thermal images appear as high-resolution colour images in real-time on a computer monitor and are recorded. The calibration of the surface temperature measurements is carried out using C-type thermocouples, which are spot-welded close to the weld region, and the data are acquired in a computer through temperature indicators over a RS485 network. The emissivity of 316LN SS plate is determined by measuring temperatures close to the weld/base metal interface, using both the thermocouple and the IR camera simultaneously at three different locations, viz. at the start, middle and end of the weld length, from which the heating and cooling cycles are generated.

Autogenous GTA welding trials were carried out on 3 mm-thick 316LN SS plates of size 125 × 50 mm^2 to prepare square-butt weld joints. The welding parameters were varied as given in Table 1 for achieving different weld bead widths and depths of penetration. A thin coating of activated flux was applied on the weld joint area prior to

Table 1 – GTA welding parameters used for IR thermography trials

Parameters	Values
Current	50–95 A
Arc voltage	12 V
Torch speed	100 mm/min
Argon gas flow rate	10 l/min

Figure 1 – Automatic GTA welding set-up

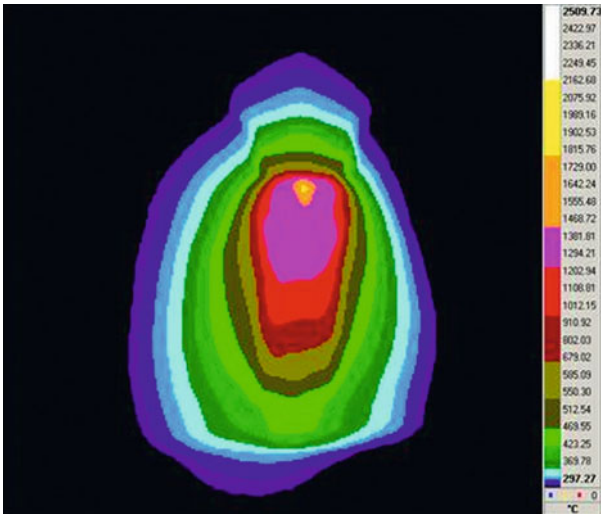

Figure 2 – Typical recomposed IR thermal image of a GTA weld pool

welding to mitigate variable weld bead penetration caused by low sulphur content (< 50 ppm). Samples cut from the welded plates at the three thermocouple locations were polished and etched to reveal the macrostructure from which the weld bead width and depth of penetration were measured using a machinists' microscope.

During these welding trials IR thermal images are acquired. To improve the accuracy of IR temperature measurements, two integration times of 230 µs and 48 µs were used for the temperature ranges of 200-600 °C and 545-1 500 °C, respectively. The recorded IR images were then recomposed to produce composite images representing the entire temperature range. Further analyses, such as spot analysis, line-scan analysis, isothermal contouring, and full-frame temperature profile analysis, of the recomposed IR images were carried out using the ALTAIR image processing software. Figure 2 shows a typical IR thermal image of a GTA weld pool.

To determine the emissivity values at the three thermocouple locations, the heating and cooling cycle data from both the sources were made to match well (Figure 3). The emissivity values estimated were 0.6, 0.44 and 0.4, respectively, at the start, middle and end of the weld. These values are in agreement with the emissivity values reported for SS, which vary in the range 0.3-0.6 in un-oxidised condition and 0.8-0.9 in oxidised condition. The temperature lag of the IR and thermocouple measurements was due to non-synchronization of triggering between the IR temperature recording and data logger for thermocouple measurement, as also the low pixel resolution (320 × 240) of the IR camera that affects the determination of exact location of thermocouple junction in the IR image.

Line-scan analysis was carried out at the same pixel value in all three frames corresponding to the three locations for weld joint, during which the respective emissivity values were used to obtain accurate temperature distributions. A typical line-scan profile and its first derivative plot are shown in Figure 4. By analysing the first derivative of the thermal profile, it is possible to identify the location of solid-liquid interface, where a change in temperature gradient occurs, due to the difference in emissivity of the solid and liquid metals. Vertical lines are drawn between the line-scan profile and the first derivative plot to identify the inflection points which corresponds to the solid-liquid interface. Thus, for any selected line-scan, the weld bead width can be computed as the distance between the two vertical lines or the distance between the left-hand-side valley and the right-hand-side peak in the first derivative

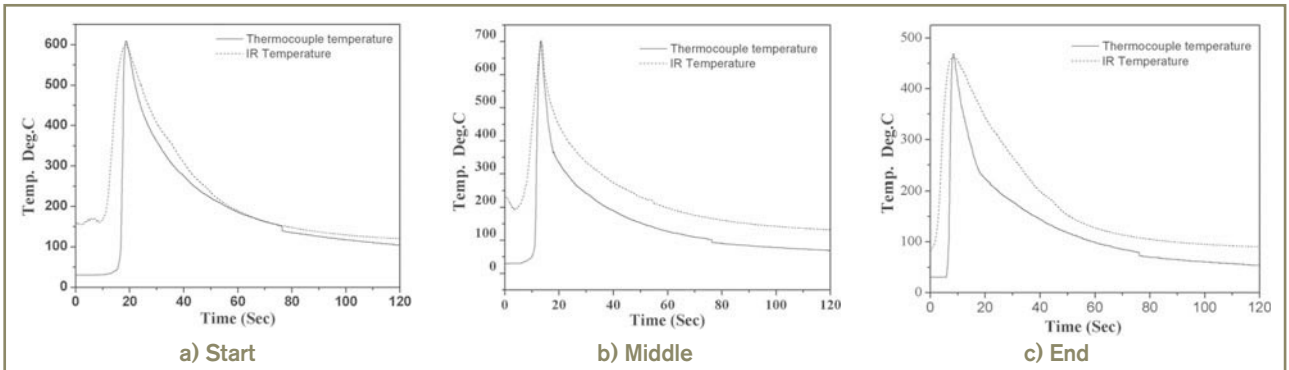

Figure 3 – Heating and cooling cycles during GTA welding measured using C-type thermocouples and IR thermography on plate surface at three weld length locations

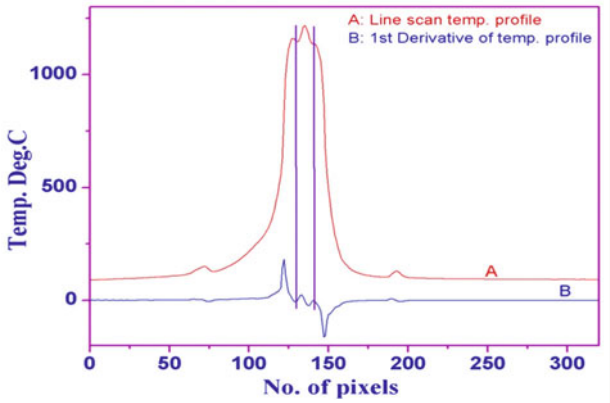

Figure 4 – Line-scan analysis for estimation of weld bead width

plot. From this the macroscopic temperature gradients can be computed as:

$$\text{Macroscopic temperature gradient} = \frac{\text{Peak temperature - Interface temperature}}{\text{Distance between peak and interface}}$$

Full-frame analysis using the ALTAIR software was carried out on the recorded IR images by the timing graph technique to obtain plots of IR intensity as a function of frame number, which were then used as IR thermal signature images for good and defective welds.

3 Results and discussion

The comparison of the actual weld bead width and the weld bead width computed by line-scan analysis of IR thermal profiles is shown in Figure 5 for the three locations of the welded joint. There is a good linear relationship between the computed (thermal) and the actual weld bead width values, with a minimum correlation coefficient of 0.8. This is in agreement with results reported in the literature [3, 5, 6].

The macroscopic temperature gradient exhibited a good inverse linear relationship with the depth of penetration of the weld bead, with a minimum correlation coefficient of 0.88 (Figure 6). The macroscopic temperature gradient increased with a decreasing depth of penetration. This is in agreement with results reported for welds of steel plates [4]. The scatter in the present data may still be due to interference from the electrode radiation on the image quality, and variation of emissivity with temperature and of the plate surface conditions. However, the present results give confidence that real-time monitoring and control of weld bead width and depth of penetration during GTA welding is feasible using IR sensing.

The temperature distribution surrounding the weld pool can be estimated from the acquired IR images of the weld pool. The temperature distribution on the plate surface for 3 mm thick square-butt weld joint of 316LN SS is shown in Figure 7.

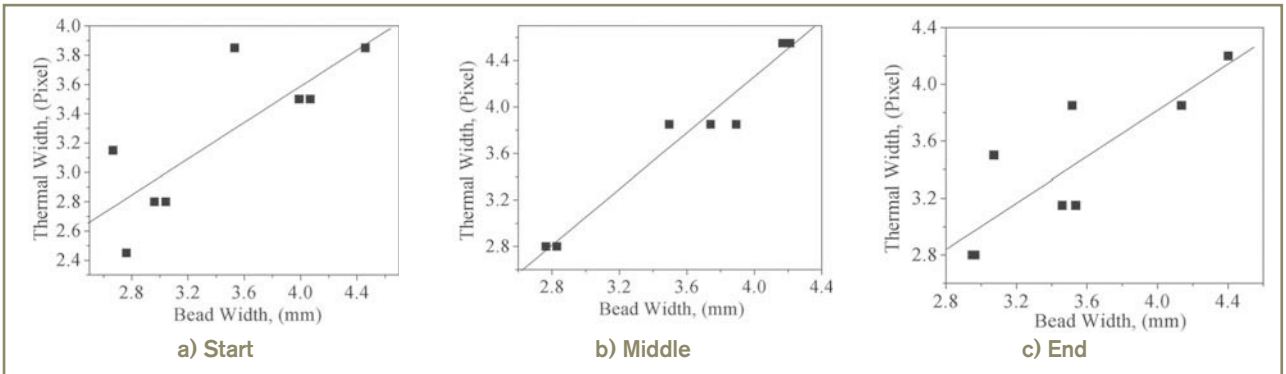

Figure 5 – Comparison between thermal (computed) and actual weld bead width at three weld length locations

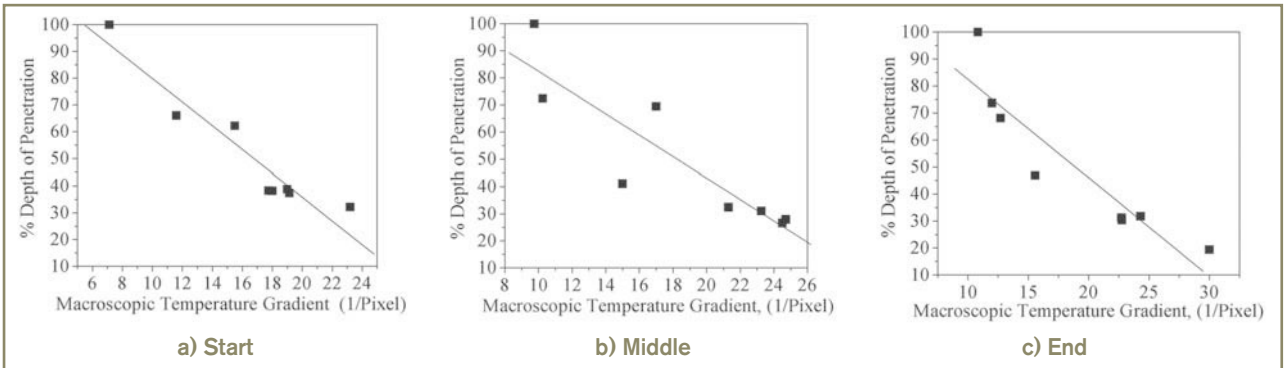

Figure 6 – Correlation between macroscopic temperature gradient and depth of penetration of weld bead at three weld length locations

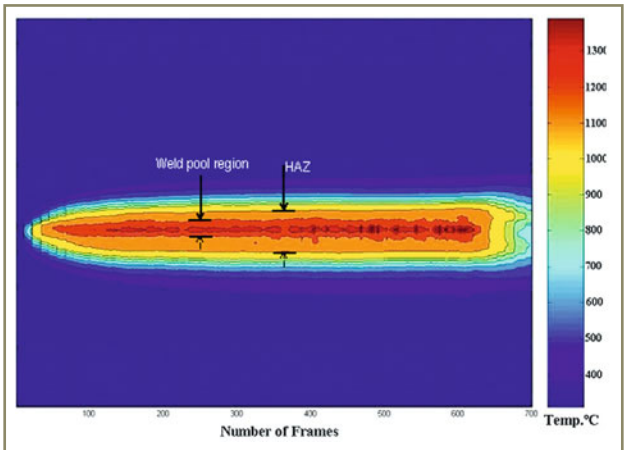

Figure 7 – Temperature distribution surrounding the weld pool on the plate surface for 3 mm-thick square-butt weld joint of 316LN SS

Each welding process has unique thermal signatures and any deviations would lead to perturbations in the surface temperature distribution, and this forms the basis for generating IR thermal signature images for welded joints of 316LN SS with and without defects.

The photograph of a welded joint without any defect and the corresponding IR thermal signature image plot is shown in Figure 8. The thermal signature image plot consists of variation in the surface temperature of the plate along the weld centre-line as a function of frame number or weld length. The temperature almost remained constant for the entire length of the weld implying that welding conditions used produced a welded joint without any defect. This thermal signature is taken as reference thermal image for a good weld.

Figure 9 shows the photograph of a welded joint with lack of fusion (LOF) weld defect with the defect area marked with a circle and the corresponding IR thermal signature image plot. Here again the defect area is marked with a circle in the plot. In the region corresponding to the LOF defect, there is a sudden drop in temperature. This is attributed to the differences in the emissivity between

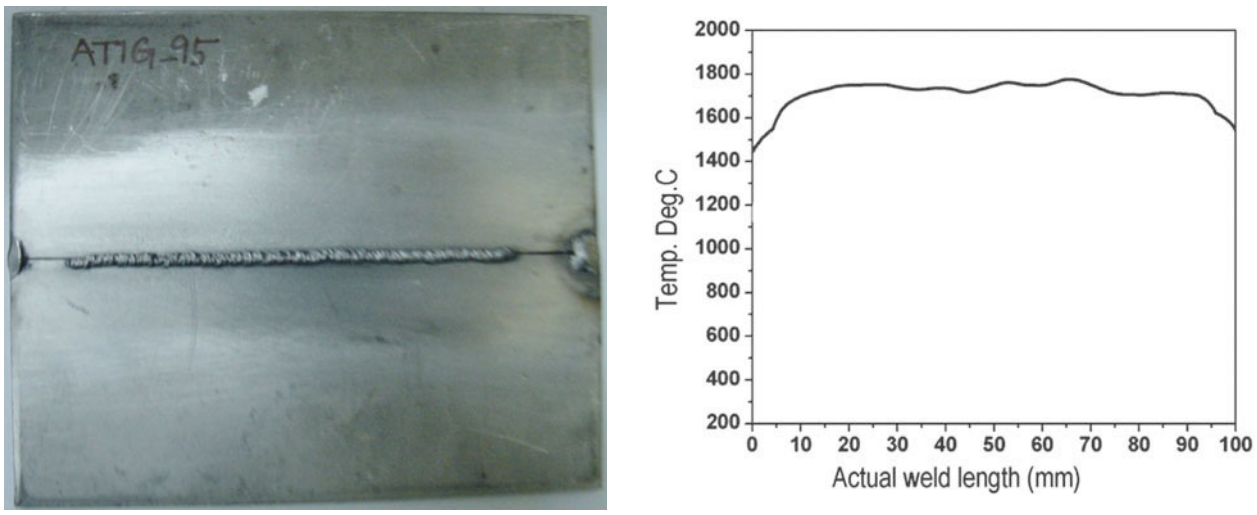

a) Photograph of welded joint without defect

b) Corresponding IR thermal signature image

Figure 8

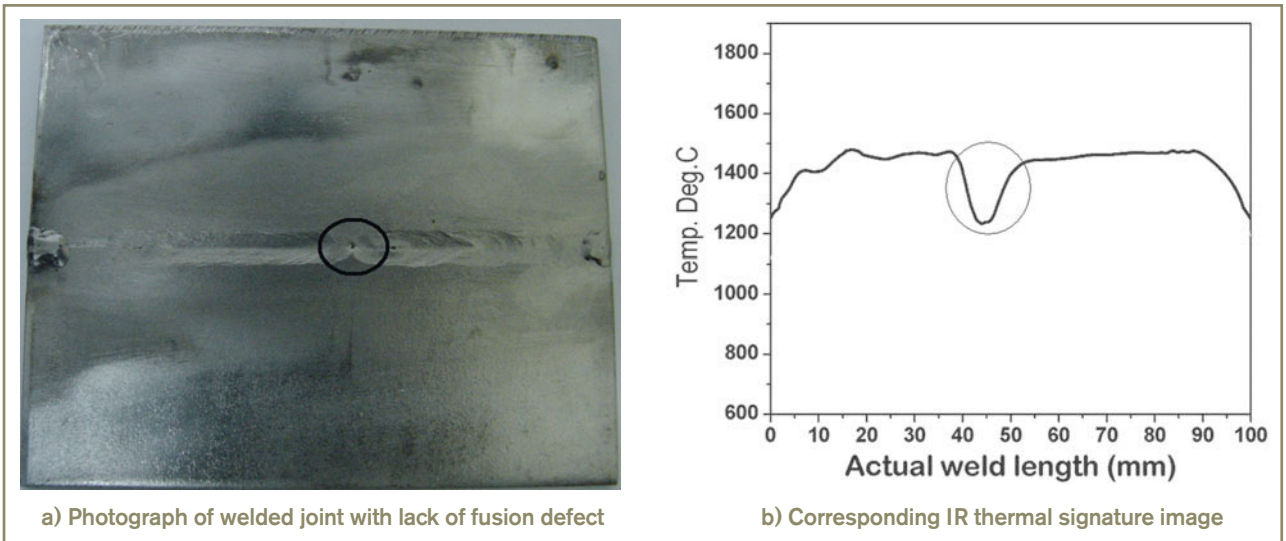

a) Photograph of welded joint with lack of fusion defect

b) Corresponding IR thermal signature image

Figure 9

the liquid and the solid, as there was no melting in this region. This image is taken as reference signature image for LOF defect. This defect was generated by shutting off the welding current for a few seconds during welding.

The photograph of a welded joint with lack of penetration (LOP) defect is shown in Figure 10 along with the corresponding IR thermal signature image plot. The defect areas are marked in the photograph as well as in the image plot. There is drop in the temperature plot for the entire length of the LOP defect. The LOP caused perturbations in the surface temperature distribution. This is taken as reference image for LOP defect. This defect was generated by varying the current throughout the welding by PLC programming.

The photograph of a welded joint with tungsten inclusion defects and the corresponding IR thermal signature image plot is shown in Figure 11. Here again the defect areas are marked in both the photograph and the image plot. At locations of tungsten inclusions, there is a definite peak in the temperature plot. These locations of tungsten inclusions were verified using X-ray radiography. The weld in the present case ends with a tungsten inclusion and hence there is a corresponding rise in the temperature at the end region of the welded joint. This image plot is taken as reference for tungsten inclusions. Small tungsten pieces were introduced into the weld pool during welding to produce this defect.

4 Conclusions

The conclusions from the present investigations are as follows.

1. A linear relationship exists between the weld bead widths computed from IR thermal profile and the actual measured values.
2. An inverse linear relationship exists between the macroscopic temperature gradient computed from the IR thermal profile and the measured depth of penetration of the weld bead.

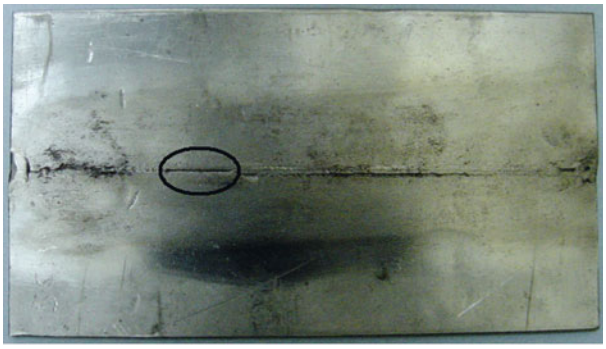

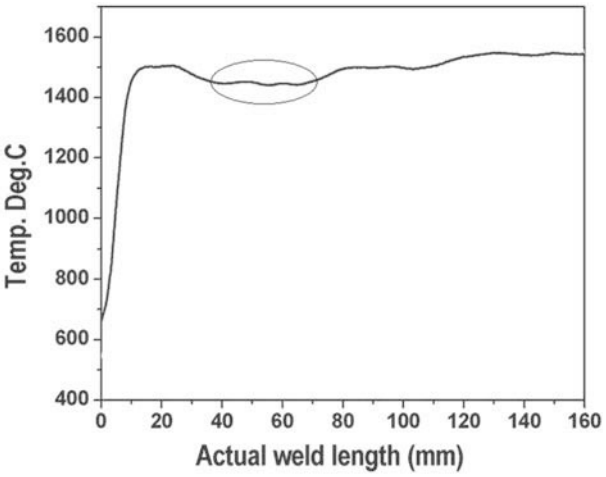

a) Photograph of welded joint with lack of penetration defect

b) Corresponding IR thermal signature image

Figure 10

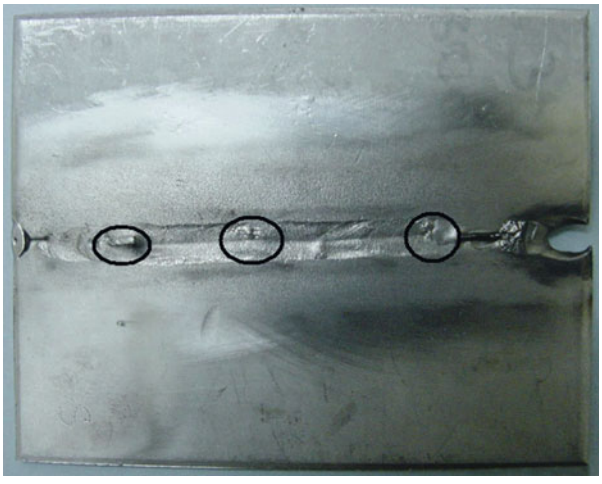

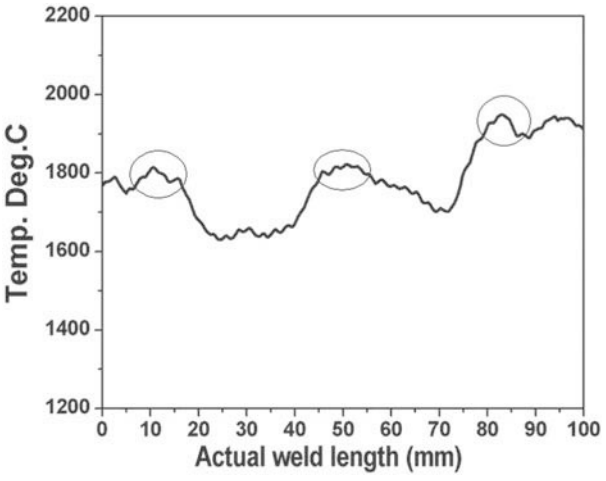

a) Photograph of welded joint with tungsten inclusion defect

b) Corresponding IR thermal signature image

Figure 11

3. Temperature distribution surrounding the weld on the plate surface can be estimated as isothermal contours of IR thermal images.
4. The IR thermal signature images generated for weld defects, such as lack of fusion, lack of penetration and tungsten inclusions can be used as reference images for on-line monitoring of weld quality using IR thermography during GTA welding of 316LN SS.
5. IR thermography is a potential tool for on-line monitoring and control of weld bead geometry during GTA welding.

Based on these investigations, a computational intelligence (CI) based control system is under development and testing for closed-loop feed-back control of depth of penetration from IR thermal images in real-time. This CI-based control system would carry out on-line correction of any deviation in the depth of penetration by adjusting the welding current in real time by sending appropriate signals to the power source through the PLC.

References

[1] Chandrasekhar N. and Vasudevan M.: Computer based operation, monitor and control of GTA welding machine and temperature measurements during welding, International Conference on Advance Manufacturing Technology, Indian National Academy of Engineering, Chennai (6-8 February 2008).

[2] Nagarajan S., Chen W.H. and Chin B.A.: Infrared sensing for adaptive arc welding, Welding Journal, 1989, vol. 68, no. 11, pp. 462s-466s.

[3] Chen W.H. and Chin B.A.: Monitoring joint penetration using infrared sensing techniques, Welding Journal, 1990, vol. 69, no. 4, pp. 181s-185s.

[4] Smith J.S. and Lucas W.: Vision based systems for controlling the arc welding operation and inspecting the weld bead profile, Welding in the World, 1999, vol. 43, Supplementary Issue, pp. 103-115.

[5] Banerjee P., Govardhan S., Wikle H.C., Liu J.Y. and Chin B.A.: Infrared sensing for on-line weld geometry monitoring and control, Journal of Engineering for Industry, 1995, vol. 117, no. 3, pp. 323-330.

[6] Menaka M., Vasudevan M., Venkataraman B. and Raj B.: Estimating bead width and depth of penetration during welding by infra-red thermal imaging, Insight, 2005, vol. 47, no. 9, pp. 564-568.

[7] Ghanty P., Vasudevan M., Mukherjee D.P., Pal N.R., Chandrasekhar N., Maduraimuthu V., Bhaduri A.K., Barat P. and Raj B.: Artificial neural network approach for estimating weld bead width and depth of penetration from infrared thermal image of weld pool, Science and Technology of Welding and Joining, 2008, vol. 13, no. 4, pp. 395-401.

[8] Balfour C., Smith J.S. and Al-Shammma A.I.: Novel edge feature correlation algorithm for real-time computer vision-based molten weld pool measurements, Welding Journal, 2006, vol. 86, no. 1, pp. 1s-8s.

[9] Al-Habaibeh A. and Parking R.: An autonomous low-cost infrared system for the on-line monitoring of manufacturing processes using novelty detection, International Journal of Advanced Manufacturing Technology, 2003, vol. 22, no. 3-4, pp. 249-258.

[10] Huang R.S., Liu L.M. and Song G.: Infrared temperature measurement and interference analysis of magnesium alloy in hybrid laser-GTA welding process, Materials Science and Engineering A, 2007, vol. 447, no. 1-2, pp. 239-243.

[11] Bicknell A., Smith J.S. and Lucas J.: Infrared sensor for top face monitoring of weld pools, Measurement Science and Technology, 1994, vol. 5, no. 4, pp. 371-378.

[12] Farson D., Richardson R. and Li X.: Infrared measurement of base metal temperature in gas tungsten arc welding, Welding Journal, 1998, vol.77, no. 9, pp. 396-401.

About the authors

Dr. Muthukumaran VASUDEVAN (dev@igcar.gov.in), Mr. Neelamegam CHANDRASEKHAR (nchandra@igcar.gov.in), Mr. Velu MADURAIMUTHU (vmm@igcar.gov.in), Dr. Arun K. BHADURI (bhaduri@igcar.gov.in) and Dr. Baldev RAJ (dir@igcar.gov.in) are all with Indira Gandhi Centre for Atomic Research, Kalpakkam (India).